

Demonstration of polarization grating imaging spectropolarimeter (PGIS)

Jihwan Kim and Michael J. Escuti

North Carolina State Univ, Dept Electrical & Computer Engineering, Raleigh, NC (USA)

ABSTRACT

We have introduced the concept of a snapshot imaging spectropolarimeter based on anisotropic diffraction gratings known as Polarization Gratings (PGs). This instrument can acquire both spectral and polarization information of an object by using the unique optical properties of PGs, which create a diffraction pattern on a single focal plane array. In this paper we develop a system matrix for reconstructing the object information from this diffraction pattern. This matrix is extendable to various configurations containing several PGs. Moreover, we demonstrate an imaging spectropolarimeter based on this approach, that was used to reconstruct both screen generated scenes and outdoor objects. Reconstructed objects are sampled at $100 \times 100 \times 51$ (x, y, λ) with 4 nm spectral resolution.

Keywords: Spectrometry, polarimetry, spectropolarimeter, imaging spectrometry, polarization grating, liquid crystals, reactive mesogens, remote sensing

1. INTRODUCTION

The purpose of our imaging spectropolarimeter is to acquire spatial (x, y), spectral (λ), and polarimetric (S_i , $i = 0, 1, 2, 3$) information from an object of interest. We previously introduced the concept of a polarization grating imaging spectropolarimeter (PGIS)¹ that used transmissive anisotropic diffraction gratings known as polarization gratings (PGs).²⁻⁴ The PGIS employs different set of PGs and Wave Plates (WPs) to make unique diffraction patterns, that are spectrally dispersed and highly polarization-sensitive, on a single Focal Plane Array (FPA). Since the spectral and polarimetric information are overlapped in the diffraction pattern, we adopt the Computed Tomography (CT) technique⁵⁻⁸ to estimate that information with iterative algorithms. This technique has been used in several non-scanning imaging systems, such as Computed Tomography Imaging Spectrometer (CTIS)⁹⁻¹¹ and Non-Scanning Computed Tomography Imaging Spectropolarimeter (NS-CTISP).¹²

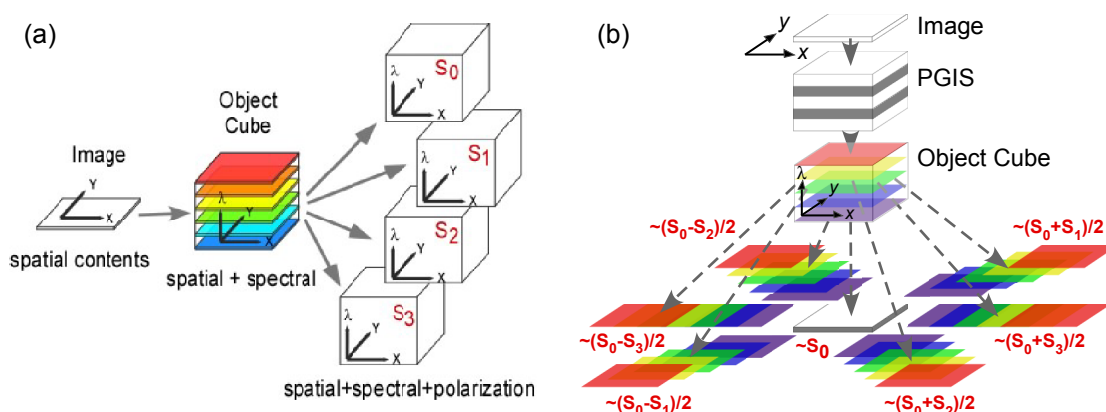


Figure 1. (a) Representation of data cubes containing spatial, spectral, and polarimetric information. (b) Conceptual design of PGIS, and diffraction pattern of an object.

Correspondence should be sent to: mjescuti@ncsu.edu, Telephone: +1 919 513 7363

2. BACKGROUND

Figure 1(a) illustrates the object cubes that conceptually represent the multi-dimensional information contained within a scene. Each object cube consists of two spatial coordinates and one spectral coordinate. The objective is to reconstruct the four cubes corresponding to the four Stokes parameters. Figure 1(b) shows the concept design of the PGIS, where dispersed image patterns are created on the FPA that are highly sensitive to the Stokes parameters of an object. PGs can diffract incident light with high efficiency into just three diffraction orders. The efficiency of the first orders is sensitive to the polarization of the incident beam, while that of the zero-order is polarization-independent. Based on these properties, the polarization response of the patterns shown above can be controlled by using combinations of PGs and WPs, as we reported before.¹³

Figure 2 shows the operation of the PGIS. Light from the object is imaged onto the FPA through the PGIS. The spatial extent of the object is controlled by the field stop. Light from the collimating lens illuminates the PGIS, where it is separated to the diffracted orders. The separation between the diffraction patterns depends upon the distance between the PGIS and the FPA, and the PG grating period which controls the diffraction angles.

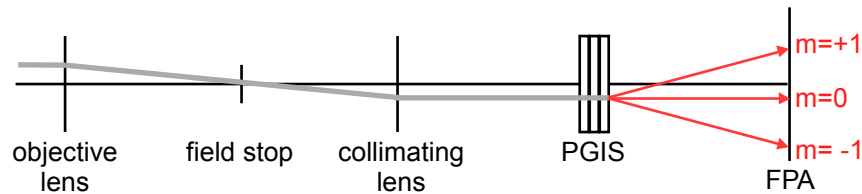


Figure 2. PGIS conceptual layout.

A PGIS benefits from the the unique properties of PGs. Unlike conventional phase or amplitude gratings, the PG operates on modulating the polarization state of incoming light and this leads to remarkable optical performance that includes $\sim 100\%$ efficiency into a single diffraction order with a good angular response. The PGs are fabricated with Liquid Crystal (LC) and photo-alignment¹⁴ materials patterned by polarization holography, for various grating periods within the visible,^{1,15,16} near-infrared,^{13,17} and midwave-infrared ranges.¹⁸ Since the intensity of the diffraction patterns from the PGs is linearly proportional to the Stokes parameters of a scene, the reconstruction process can be done without any post-processing, which otherwise limits the spectral resolution and detection speed. In order to make well-separated diffraction patterns that are essential for computed tomography reconstruction, PGs can be easily stacked into various configurations, as we have demonstrated with a prototype nonmechanical beam steering system¹⁷ based on stacked PGs and WPs.

3. PGIS INSTRUMENT

3.1 PGIS Mathematical Model

The PGIS is a snapshot imaging spectropolarimeter that needs no moving parts or scanning processes. In this system, the spatial, spectral, and polarization information of the scene is allowed to overlap in a two-dimensional plane and collected on a single FPA. A continuous model of the PGIS can be rewritten as:

$$g(\mathbf{r}') = \sum_{j=1}^{\infty} \sum_{i=0}^3 \int \int \int f(\mathbf{r}, \lambda, i) h(\mathbf{r}, \lambda, i : \mathbf{r}'_j) d^2 \mathbf{r} d\lambda + n(\mathbf{r}'). \quad (1)$$

where the projection $g(\mathbf{r}')$ and the object cube $f(\mathbf{r}, \lambda, i)$ are continuous functions of their arguments. Here i denotes the different Stokes object cubes ($i = 0, 1, 2, 3$), and j accounts for multiple diffraction patterns. Also $h(\mathbf{r}, \lambda, i : \mathbf{r}'_j)$ is a transfer function which contains geometric mapping information between object cubes and projections, with spectral and polarimetric responses. Assuming that collimated light comes into the PGIS, a diffraction displacement vector can be described as follows.¹

$$\mathbf{d}_{m,j}(\lambda) = L \cdot \tan(\sin^{-1}(m\lambda/\Lambda)) \cdot \hat{\mathbf{r}}'_j, \quad (2)$$

Here L is the distance between the PGIS and the FPA, and $m = 0, \pm 1$ is the diffraction order. Λ is the grating period, and $\hat{\mathbf{r}}'$ is a unit vector that defines the azimuth angle of j^{th} diffraction pattern. Let $I_{k,m}$ represent the intensity corresponding to the PG and WP combination denoted by k ($k = 1, 2, 3$), and the m^{th} diffraction order ($m = 0, \pm 1$). Here $k = 1$ refers to a combination of two WPs with slow axes at 0° and $+45^\circ$ followed by the PG. When $k = 2$, there is only one WP with slow axis at 0° followed by the PG while $k = 3$ is the case with just the PG alone. If we consider these arrangements, the following relations are true for the orders of interest:

$$I_{k,0} \propto S_0, \quad (k = 1, 2, 3), \quad (3a)$$

$$I_{1,\pm 1} \propto \frac{1}{2}(S_0 \mp S_1), \quad (3b)$$

$$I_{2,\pm 1} \propto \frac{1}{2}(S_0 \pm S_2), \quad (3c)$$

$$I_{3,\pm 1} \propto \frac{1}{2}(S_0 \mp S_3) \quad (3d)$$

where S_i is a Stokes parameter ($i = 0, 1, 2, 3$). Using additional Dirac- δ functions,¹⁹ the transfer function can be derived as:

$$h(\mathbf{r}, \lambda, i : \mathbf{r}'_j) = \delta\{\mathbf{r}'_j - (\mathbf{r} + \mathbf{d}_{m,j}(\lambda))\} \left\{ \frac{1}{2} \delta(k - i) + \frac{1}{2} \right\} \eta(\lambda). \quad (4)$$

where the first term indicates geometric mapping, and the second term includes polarization response for different patterns k . Here $\eta(\lambda)$ denotes the spectral transmittance, which is dominated by a spectral efficiency of the PGs and that of the camera.

The system function can now be described as:

$$g(\mathbf{r}') = \sum_{j=1}^{\infty} \sum_{i=0}^3 \int \int \int f(\mathbf{r}, \lambda, i) \delta\{\mathbf{r}'_j - (\mathbf{r} + \mathbf{d}_m(\lambda))\} \left\{ \frac{1}{2} \delta(k - i) + \frac{1}{2} \right\} \eta(\lambda) d^2 \mathbf{r} d\lambda + n(\mathbf{r}'), \quad (5)$$

where k indicates the four diffraction patterns of interest. This continuous function provides the analytic relationship between multi-dimensional object cubes and projection on the FPA.

While the system function can be described in a continuous manner, the object cubes and projections should be considered discrete, since all projection data is from the discrete sensor arrays, and is related to the corresponding discrete volumetric units of the object cubes. Analogous to a pixel being the smallest data unit on a sensor array, a volumetric data unit (voxel) can be considered in object cubes. The relationship between an object vector \mathbf{f} having voxels and \mathbf{g} containing pixels can be described by the system matrix \mathbf{H} , which contains all of the geometric mapping information, along with spectral and polarimetric responses. The system function is now transformed to the following, with the noise-free assumption for simplicity:

$$\mathbf{g} = \mathbf{H} \mathbf{f}, \quad (6a)$$

$$\mathbf{g} = [\mathbf{g}_1 \ \mathbf{g}_2 \ \mathbf{g}_3]^T, \quad (6b)$$

$$\mathbf{f} = [\mathbf{f}_0 \ \mathbf{f}_1 \ \mathbf{f}_2 \ \mathbf{f}_3]^T, \quad (6c)$$

Here \mathbf{g}_k is the $M_k \times 1$ projection vector for pattern k , (M_k is the number of pixels on pattern k), and \mathbf{f}_i is $N \times 1$ object vector of the S_i Stokes parameter cube. N is the number of voxels in a single object cube; for example, $N=10^6$ when object cube is sampled at $100 \times 100 \times 100$ (x,y, λ). In order to represent the system matrix \mathbf{H} , a response mapping matrix of pattern k , \mathbf{W}_k , can be defined as:

$$\mathbf{W}_k = \begin{bmatrix} w_{1,1} & w_{1,2} & \cdots & w_{1,N} \\ w_{2,1} & w_{2,2} & \cdots & w_{2,N} \\ \vdots & \vdots & \ddots & \vdots \\ w_{M_k,1} & w_{M_k,2} & \cdots & w_{M_k,N} \end{bmatrix}, \quad (7a)$$

$$\mathbf{Z}_k = \mathbf{0}_{M_k, N}, \quad (7b)$$

where \mathbf{W}_k is the $M_k \times N$ matrix that represents the linear mapping from voxels in the object cube \mathbf{f}_i to the projection \mathbf{g}_k , and entry $w_{a,b}$ is spectral response of voxel(b) in object cubes and pixel(a) on a sensor array. \mathbf{Z}_k is a zero matrix with all entries being zero, and the size of \mathbf{Z}_k is the same as \mathbf{W}_k ($M_k \times N$). Then, the system matrix \mathbf{H} can be written with block partitioned matrices, \mathbf{W}_k and \mathbf{Z}_k .

$$\mathbf{H} = \begin{bmatrix} \mathbf{W}_1 & \mathbf{W}_1 & \mathbf{Z}_1 & \mathbf{Z}_1 \\ \mathbf{W}_2 & \mathbf{Z}_2 & \mathbf{W}_2 & \mathbf{Z}_2 \\ \mathbf{W}_3 & \mathbf{Z}_3 & \mathbf{Z}_3 & \mathbf{W}_3 \end{bmatrix}, \quad (8)$$

\mathbf{H} is a M -by- $4N$ matrix ($M = \sum_{k=1}^3 M_k$) whose number of rows represents the total number of pixels on the FPA and the number of columns indicates total number of voxels in object cubes.

$$\begin{bmatrix} \mathbf{g}_1 \\ \mathbf{g}_2 \\ \mathbf{g}_3 \end{bmatrix} = \begin{bmatrix} \mathbf{W}_1 & \mathbf{W}_1 & \mathbf{Z}_1 & \mathbf{Z}_1 \\ \mathbf{W}_2 & \mathbf{Z}_2 & \mathbf{W}_2 & \mathbf{Z}_2 \\ \mathbf{W}_3 & \mathbf{Z}_3 & \mathbf{Z}_3 & \mathbf{W}_3 \end{bmatrix} \begin{bmatrix} \mathbf{f}_0 \\ \mathbf{f}_1 \\ \mathbf{f}_2 \\ \mathbf{f}_3 \end{bmatrix} \quad (9)$$

From the practical point of view, the length of columns \mathbf{g} and \mathbf{H} can be extended according to the size of projection patterns, which generally improves the estimate of \mathbf{f} . For example, the length of the matrix would be doubled if the objects were estimated with doubled diffraction patterns on the FPA.

3.2 Reconstruction Algorithm

The object cube \mathbf{f} is reconstructed from the projected diffraction patterns \mathbf{g} on FPA by means of an iterative algorithm known as MART.^{20,21} The initial estimation, f^0 is the spectrally uniform zeroth order that is used for the following estimation of f^l , where l is the iterative index.

$$\text{MART} : \hat{f}_n^{(l+1)} = \hat{f}_n^{(l)} \frac{(\mathbf{H}^T \mathbf{g})_n}{(\mathbf{H}^T \mathbf{H} \hat{\mathbf{f}}^{(l)})_n} \quad (10)$$

The iterative algorithms require large computational time to acquire relatively higher resolution, but they are still attractive for snapshot imaging systems.

3.3 System Calibration

The system matrix \mathbf{H} contains the spectral response and geometric mapping information between a voxel in the object cubes and a pixel on the FPA. Since we assumed a linear system, this information can be estimated based on the system parameters such as focal length of imaging lens, and the diffraction properties of PGs. However, in real situations, the geometric mapping may not be easily calculated. For example, misalignment of lenses and camera can dislocate each projection pattern, and the aberration of lenses may cause further distortion. In order to calibrate the geometric mapping information of the system, projection distance, $\mathbf{d}_m(\lambda)$ of selected voxels, was measured with various light sources having a single wavelength (HeNe 633nm, Nd:YAG 532nm) and narrowband wavelength range (FWHM < 10nm, 400nm ~ 700nm).

Figure 3(a) shows a sample calibration image containing the position of diffracted beams of two single wavelength sources (633nm and 532nm). The spots were collected at the center of the FPA and denote the relative distances between the zero and first diffraction orders. System matrix \mathbf{H} was revised based on this mapping information and several sample spots were used to make it more reliable. For wavelengths where information was difficult to acquire, data from neighboring wavelengths was interpolated. In this paper, we used simple PGIS design (Figure 3(b)) that creates nine diffraction patterns. Each pattern has different polarization

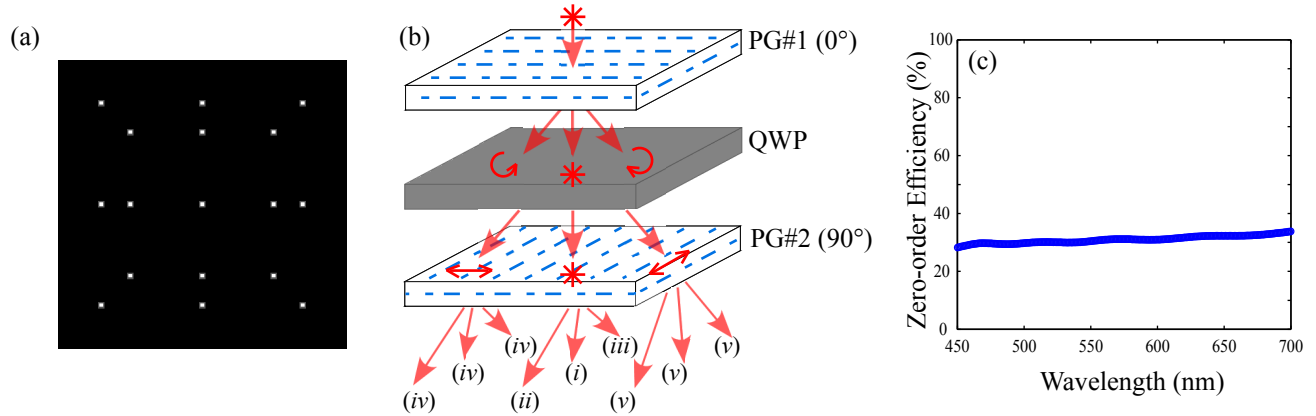


Figure 3. (a) Projection image on a FPA with two different light sources (532nm and 633nm); (b) PGIS design configuration with 2 PGs and a WP; (c) Zero-order diffraction efficiency of PGs

sensitivity; for example, (i) is the global zero order, (ii),(iii) are related to pattern 2 ($k = 2$), and (iv),(v) are related to pattern 3 ($k = 3$). From this design, three Stokes parameters (S_0, S_2 , and S_3) can be estimated within visible range, and the design can be extended with one additional PG and WP, to extract full Stokes parameters including S_1 .

Polarization sensitivity of the patterns varies according to the path of rays, and the spectral responses of each diffraction order. As shown in Figure 3(c), $\sim 30\%$ diffraction efficiency of PGs²² is chosen to separate incoming light to several diffraction patterns with equal power to prevent saturation in a specific order, and to increase the signal to noise ratio. Based on the calibration information, the system matrix \mathbf{H} can be modified with tested mapping information and polarization responses. Here, we used a few light sources to check the projection images. This mapping can be improved with the use of broadband sources and spectrometers, to acquire more spectrally varied geometric and polarization responses of each object cube.

4. EXPERIMENTAL RESULTS

The previous simulation results¹ showed that PGIS could reconstruct spectral and polarization information of images by using stacks of PGs and WPs without significant errors. Such a reconstruction is possible for an object having variable spatial, spectral, and polarimetric content. In this paper as proof of concept, we built a compact imaging system using off-the-shelf lenses and an iris acting as a field stop. To capture the diffraction patterns, we used a 8-bit monochromatic machine vision camera (Thorlab) operating in the visible range. To test this system, we first used images from a LCD monitor as the target.

4.1 Indoor Test

In order to manipulate the spectral and polarimetric information of an image, we generated some simple targets on a LCD monitor. Figure 4(a) shows one such target image where each color dot has different spectral and polarimetric information. Polarization of the light from these dots was controlled by attaching linear polarizer and QWPs in front of the monitor as follows: (i) red (peak at 600nm) dot has a linear polarizer with axis at -45° for $S_2 = -1$, (ii) green (peak at 540nm) dot has a polarizer at -45° and a QWP (0° axis) for $S_3 = +1$, and the (iii) yellow (peak at 540nm and 600nm) has the polarizer at -45° and QWP (90° axis) for $S_3 = -1$. Diffraction pattern of this image captured by the monochromatic camera contained 9 dispersion images as shown in figure 4(b). The panchromatic image found in the zero order, contains the intensity profile of the target image. Other dispersions show different characteristics because the PGIS diffracts incoming beams into high orders with

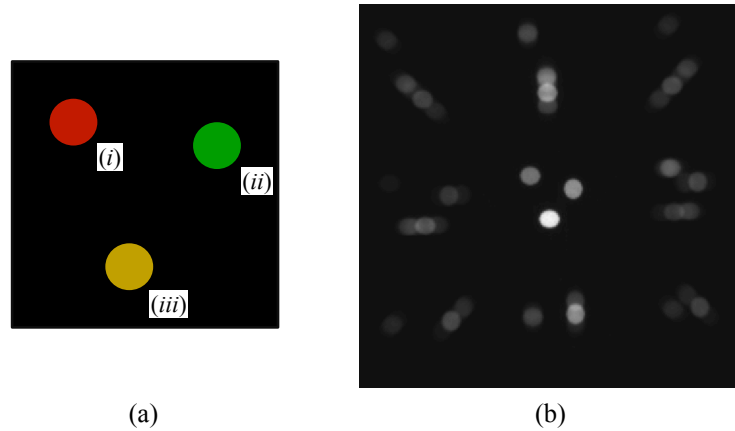


Figure 4. (a) Target image; (b) Diffraction pattern on FPA (400×400).

different efficiency, that is governed by polarization information in the target. Spatial resolution (100×100) of the reconstructed images was determined by size of zero order pattern on CCD while the spectral resolution (4 nm) was selected depending upon the dispersion length of the target.

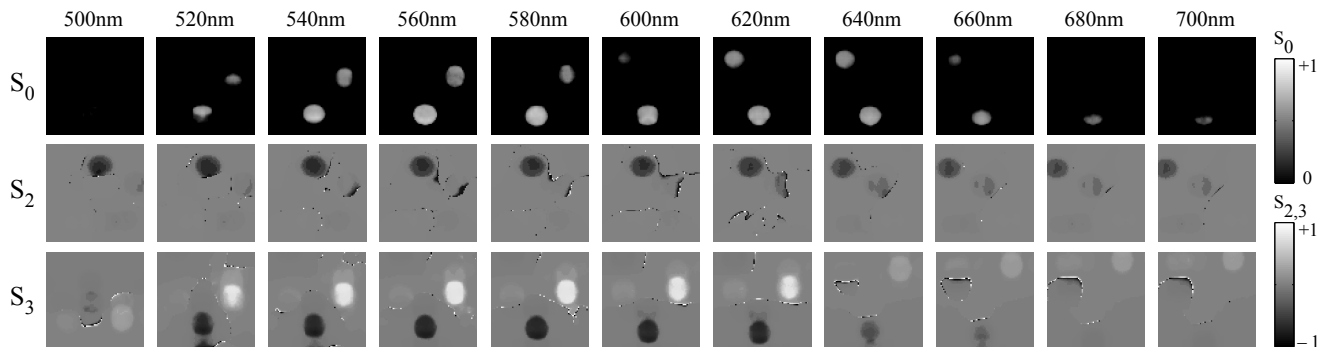


Figure 5. Reconstructed Stokes images in the range of 500nm to 700nm (the figure only shows 11 of 51 spectral band reconstruction).

Figure 5 shows the reconstructed data cubes from the diffraction patterns with 51 spectral bands within the 500-700 nm range, and 100×100 spatial resolution (10^4 pixels). Here only 11 of these 51 reconstructed bands are shown. The first row contains the S_0 reconstruction that only has the spectral information of the object. The second and third rows are the reconstructed S_2 and S_3 images respectively. Bright regions in these rows represent positive information while the dark regions represent negative data. Here we can see good correlation between the actual object data and the reconstructed information. For example, the reconstructed S_3 values match exactly in the corresponding wavelength range, to that of the original object.

Figure 6(a) compares this above reconstructed data with normalized data measured with an integrating sphere connected to a spectrometer. Here we compare the S_0 parameter in the red and green regions. We can see a reasonable match between the two sets of data. In (b), (c) we plot the S_2, S_3 parameters for the red and green dots respectively. Once again we see that S_2 and S_3 assumes the corresponding sign as expected.

4.2 Outdoor Test

Similar to the target objects on the LCD monitor, we also tried to reconstruct outdoor objects with the same PGIS parameters. Since the imaging system was calibrated for the indoor test, the same geometric and spectral information of system matrix H could be used for outside objects.

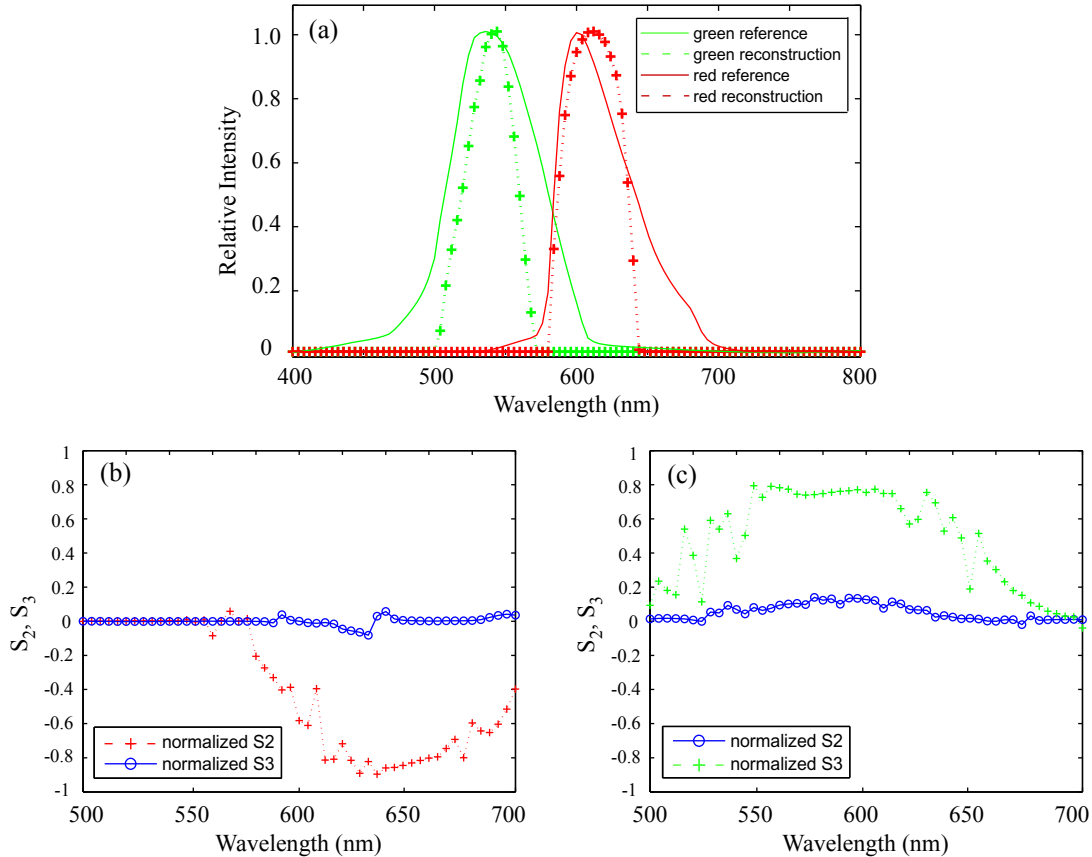


Figure 6. Reconstructed spectra from two different locations of red and green dots: (a) Spectra of S_0 for two regions. Solid lines denote the comparison spectra measured with a reference spectrometer; (b) Normalized S_2 and S_3 spectra of red dot region; (c) Normalized S_2 and S_3 spectra of green dot region.

To extract polarization information from the PGIS, we used a narrowband (FWHM < 10nm) filter to reduce the dispersion in the diffraction patterns. Part (a) of Figure 7 shows the two reconstruction targets in an outdoor image. For better spatial resolution, different PGs having higher diffraction angles were used, and the spatial resolution was increased to 250×250 . The first column in parts (b), (c) shows the reconstructed S_0 parameter corresponding to the intensity profile in the range of the color filter (peak at 550nm). The second column shows the normalized Stokes parameter S_3/S_0 for the same targets, while the third column gives the Degree Of Circular Polarization (DOCP).

Even in this narrow spectral range, especially when we look at the last column, man made objects such as the targets in this case appear distinctly different from the background. In fact details that are hidden in the S_0 column are revealed in the second and third columns. The quality of reconstructed images can be improved by increasing the resolution of the camera used. The spectral resolution can be improved by using PGs with smaller periods that provide more dispersion in the diffraction patterns. In this simple demonstration, the PGIS consisted of only two PGs and one WP. But several other configurations of PGs and WPs that may offer other advantages, need to be tested further.

5. CONCLUSIONS

We have introduced the concept of Polarization Grating based Snapshot Imaging Spectropolarimetry (PGIS). We employ multiple PGs to create chromatic dispersion patterns that are linearly proportional to Stokes vectors (polarization information) embedded in a target object. We demonstrated an imaging system which produces a 2D projection of an object containing spatial, spectral and polarization information. For initial tests, the spatial,

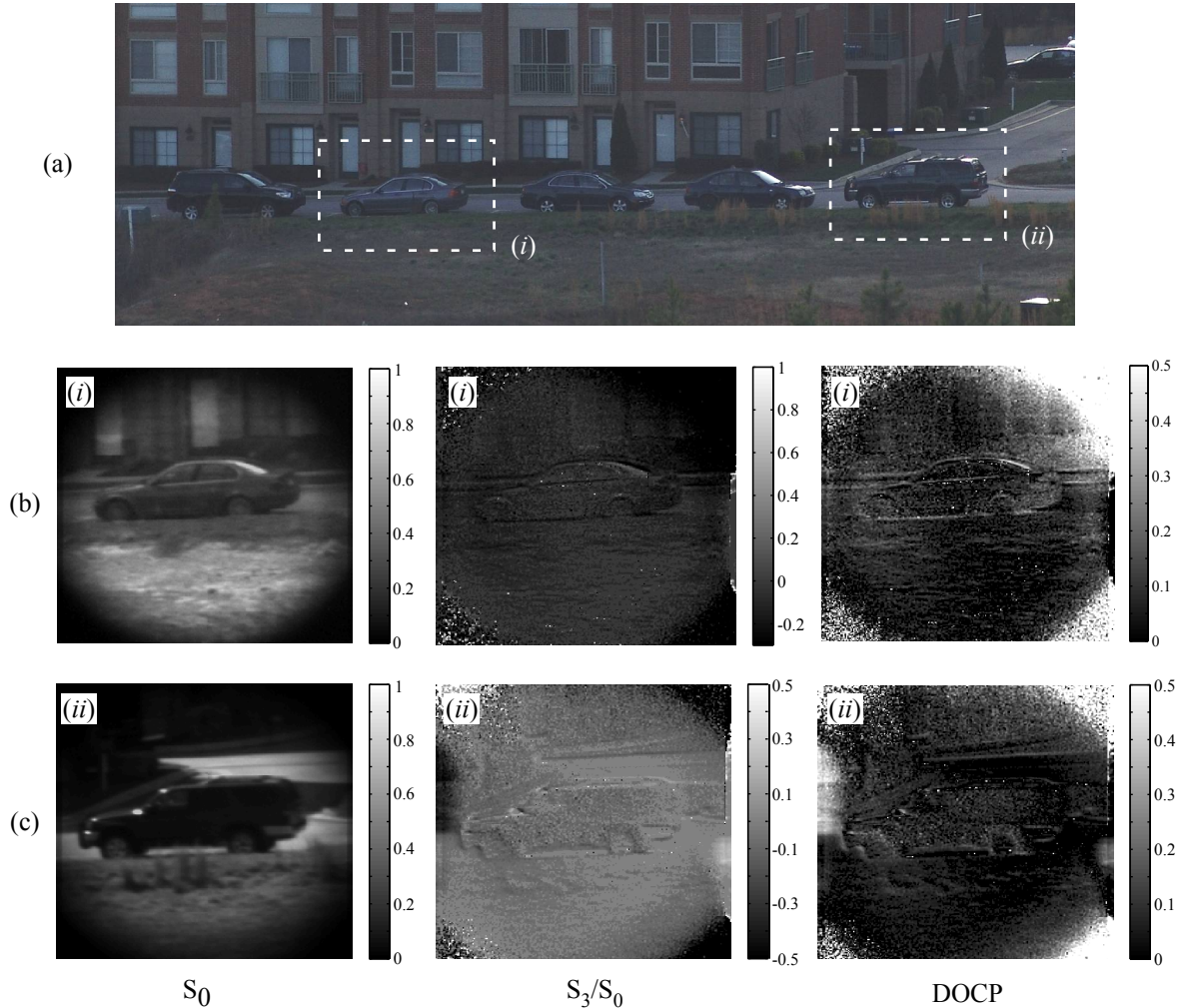


Figure 7. (a) Targets (i) and (ii) in outdoor image for reconstruction. Reconstructed S_0 , S_3/S_0 , and DOCP for (b) Target (i), and (c) (ii) respectively.

spectral and polarimetric information of simulated images was successfully reconstructed using this approach. PGIS may have capability to reconstruct the object with higher resolution in all dimensions, since it can estimate 4D object data from the dispersion patterns without Fourier-domain post-processing, and may allow a faster overall reconstruction than current snapshot imaging approaches. We continue to develop a more optimal and practical PGIS approach by studying several other promising configurations.

ACKNOWLEDGMENTS

The authors gratefully acknowledge support from the National Science Foundation (grant ECCS-0621906).

REFERENCES

- [1] Kim, J. and Escuti, M. J., "Snapshot imaging spectropolarimeter utilizing polarization gratings," *Proc. SPIE* **7086**, 708603 (2008).
- [2] Crawford, G. P., Eakin, J. N., Radcliffe, M. D., Callan-Jones, A., and Pelcovits, R. A., "Liquid-crystal diffraction gratings using polarization holography alignment techniques," *J. of Appl. Phys.* **98**, 123102 (2005).

- [3] Nikolova, L. and Todorov, T., "Diffraction efficiency and selectivity of polarization holographic recording," *Optica Acta* **31**, 579–588 (1984).
- [4] Tervo, J. and Turunen, J., "Paraxial-domain diffractive elements with 100% efficiency based on polarization gratings," *Opt. Lett.* **25**, 785–786 (2000).
- [5] Okamoto, T. and Yamaguchi, I., "Simultaneous acquisition of spectral image information," *Opt. Lett.* **16**, 1277–1279 (1991).
- [6] Gordon, R., "A tutorial on art (algebraic reconstruction technique)," *IEEE Trans. on Nuclear Science* **21**, 78–93 (1974).
- [7] Kak, A. C. and Slaney, M., [*Principles of computerized tomographic imaging*], IEEE Press (1998).
- [8] Bertero, M. and Boccaci, P., [*Introduction to inverse problems in imaging*], Institute of Physics Pub. (1998).
- [9] Descour, M. and Dereniak, E., "Computed-tomography imaging spectrometer - experimental calibration and reconstruction results," *Appl. Opt.* **34**, 4817–4826 (1995).
- [10] Volin, C. E., Garcia, J. P., Dereniak, E. L., Descour, M. R., Hamilton, T., and McMillan, R., "Midwave-infrared snapshot imaging spectrometer," *Opt. Eng.* **40**(25), 4501–4506 (2001).
- [11] Johnson, W. R., O'Connell, D., Dereniak, E. L., and Hege, E. K., "Novel calibration recovery technique for an expectation maximization tomographic reconstruction," *Opt. Eng.* **43**, 10–11 (2004).
- [12] Miles, B. H. and Kim, L. B., "Non-scanning computed tomography imaging spectroplarimeter (ns-ctisp) design and calibration," *Proc. SPIE* **5432**, 155 (2004).
- [13] Escuti, M. J., Oh, C., Sanchez, C., Bastiaansen, C., and Broer, D. J., "Simplified spectropolarimetry using reactive mesogen polarization gratings," *Proc. SPIE* **6302**, 632614 (2006).
- [14] Crawford, G. P., Eakin, J. N., Radcliffe, M. D., Callan-Jones, A., and Pelcovits, R. A., "Liquid-crystal diffraction gratings using polarization holography alignment techniques," *J. Appl. Phys.* **98**, 123102 (2005).
- [15] Escuti, M. J. and Jones, W. M., "A polarization-independent liquid crystal spatial light modulator," *Proc. SPIE* **6332**, 63320M (2006).
- [16] Komanduri, R. K., Jones, W. M., Oh, C., and Escuti, M. J., "Polarization-independent modulation for projection displays using small-period LC polarization gratings," *J. SID* **15**, 589–594 (2007).
- [17] Kim, J., Oh, C., Escuti, M. J., Hosting, L., and Serati, S., "Wide-angle nonmechanical beam-steering using thin liquid crystal polarization gratings," *Proc. SPIE* **7093**, 709302 (2008).
- [18] Packham, C., Escuti, M. J., Boreman, G., Quijano, I., Ginn, J. C., Franklin, B., Axon, D. J., Hough, J. H., Jones, T. J., Roche, P. F., Tamura, M., Telesco, C. M., Levenson, N., Rodgers, J. M., and McGuire, J. P., "Design of a mid-ir polarimeter for sofia," *Proc. SPIE* **7014**, 70142H (2008).
- [19] Chiu, M. Y. and Barrett, H. H., "Three-dimensional radiographic imagign with a restricted view angle," *J. Opt. Soc. Am.* **83**, 325–330 (1979).
- [20] Byrne, C. L. and Graham-Eagle, J., "Image iterative reconstruction algorithms," *Proc. SPIE* **1767**, 83–92 (1992).
- [21] Lent, A., "A convergent algorithm for maximum entropy image restoration with a medical x-ray application," *Soc. Phot. Sci. and Eng.* , 249–257 (1976).
- [22] Oh, C. and Escuti, M. J., "Achromatic diffraction from polarization gratings with high efficiency," *Opt. Lett.* **33**, 2287–2289 (2008).